Quantum Electronics **46** (11) 1002–1008 (2016)

DOI: 10.1070/QEL16190

Filamentation of an annular laser beam with a vortex phase dislocation in fused silica

E.V. Vasil'ev, S.A. Shlenov

Abstract. **The filamentation of a femtosecond laser pulse in fused silica has been numerically investigated for the case of an annular beam with a phase singularity at a wavelength of 800 nm. The spatiotemporal propagation dynamics of the pulse and the transformation of its frequency-angular spectra are analysed. It is shown that a tubular structure with a radius of 3–4 μm, peak intensity of about 2.4×10^{13} W cm^{-2}, and maximum plasma density on the order of 10^{20} cm^{-3} is formed in the nonlinear focus; the length of this structure significantly exceeds the waist length in the linear case. The results of the analysis are compared with the data obtained for an annular beam free of phase dislocations and for a Gaussian beam.**

Keywords: *filamentation, optical vortex, phase singularity, annular beam.*

1. Introduction

The propagation of a high-power femtosecond laser beam in transparent dielectrics is a highly nonlinear process, during which the light field energy can be localised in the form of a thin high-intensity structure (filament), which is retained at a distance of many diffraction lengths [1–3]. The filament formation is mainly due to the influence of Kerr self-focusing and defocusing in a plasma channel, self-induced as a result of the nonlinear photoionisation of the medium. The mutual competition between these effects maintains the quasi-waveguide regime of laser pulse propagation in a nonlinear medium. A necessary condition for the formation of a femtosecond filament is as follows: the peak pulse power must exceed the threshold value P_{cr}, which depends on the beam wavelength, beam shape and the parameters of the medium. According to different sources, the critical self-focusing power for a Gaussian beam with a wavelength of 800 nm in air is 2–6 GW [4]. In solid dielectrics, this value decreases to several megawatts ($P_{cr} \approx 2.7$ MW in fused silica [5]).

Filamentation is of interest for many applications. Radiation self-channeling in gases can be used in environment sensing [6], filament-induced breakdown spectroscopy [7], and design of dynamic microwave waveguides [8]. High power density in a filament makes it possible to carry out micromodifications of solid dielectrics without their thermal decomposition [9].

The presence of a phase singularity in a beam may not only increase the critical self-focusing power [10] but also significantly affect the character of pulse propagation in a medium. In particular, the formation of an annular spatial structure during filamentation of beams with a phase singularity on their axis can in principle be used to form tubular micromodifications in solid dielectrics.

The possibility of using optical vortices specifically to delay the multiple filamentation onset was demonstrated in [11]. An analysis (by means of the perturbation method and numerical calculations) predicted an increase by an order of magnitude in the distance to the start point of multiple filamentation in a vortex beam with a relative noise intensity of 10% in comparison with super-Gaussian and annular beams.

Beams with vortex phase singularities can experimentally be obtained in different ways. In the case of femtosecond radiation, it is important to provide conditions for the occurrence of an optical vortex in a wide spectral range. To this end, one can use uniaxial crystals, where beams with vector singularities are formed due to the birefringence [12]. An optical system consisting of two uniaxial crystals with mutually perpendicular axes and a polariser transforms a circularly polarised light beam into a singular beam [13, 14].

Apparently, filamentation of vortex beams was observed for the first time in [15]. Annular beams with a phase singularity on their axis propagated in sodium vapours to be self-focused and form a high-intensity ring, which was then decomposed into separate hot points due to the azimuthal modulation instability. However, the break of the axial symmetry and beam decomposition into separate fragments may occur at a rather large distance. For example, it was experimentally and numerically shown in [16] that the primary self-focusing of an annular beam with a phase singularity in air is followed by the formation of a high-intensity ring, which induces photoelectrons of plasma. This tubular shape is retained up to distances on the order of several hundreds of metres, after which it decomposes because of the modulation instability.

It was shown in [17] by an example of optical vortices with a topological charge $m = \pm 1$ that, at sufficiently small initial amplitude–phase perturbations of the initial pulse, the stable propagation distance of the optical vortex exceeds the nonlinear focusing length.

Along with the problems of spatial stability of the filament formation in beams with phase dislocations, the characteristics and specific features of the transformation of propagating-beam frequency spectrum are also of great interest. Neshev et al. [18] experimentally observed supercontinuum

E.V. Vasil'ev, S.A. Shlenov Faculty of Physics, M.V. Lomonosov Moscow State University, Vorob'evy gory, 119991 Moscow, Russia; International Laser Center, M.V. Lomonosov Moscow State University, 119991 Vorob'evy gory, Moscow, Russia; e-mail: vasilev.evgeniy@physics.msu.ru

Received 4 August 2016; revision received 19 September 2016
Kvantovaya Elektronika **46** (11) 1002–1008 (2016)
Translated by Yu.P. Sin'kov

generation with conservation of the annular shape of a beam with a phase dislocation and measured the pressure dependence of the supercontinuum bandwidth in argon [19].

The numerical calculations based on the approximation of slowly varying amplitude, performed in [17] for beams with the same peak power, showed the broadening of the frequency-angular spectrum of annular beams with a phase singularity under filamentation in air to exceed that for Gaussian beams. These results cannot be directly generalised to the case of solid dielectrics, where one must take into account collisions during ionisation evolution in the femtosecond-pulse plasma channel. In addition, the description of the spectral broadening must be performed with due regard to the self-sharpening of pulse edges.

In this paper, we report the results of studying the femtosecond filamentation during propagation of annular beams with a phase singularity in fused silica in the range of normal group-velocity dispersion at a wavelength of 800 nm. Numerical experiments were performed with allowance for the effects of wave nonstationarity within the slowly varying wave approximation [20]. A comparative analysis of the spatiotemporal dynamics of radiation and its frequency-angular spectra is performed for these beams, an annular beam free of phase dislocation, and a Gaussian beam, provided that they have the same power.

It is shown that the self-action in the optical vortex can lead to the tubular filament formation. In this case, the frequency-angular spectrum of the pulse acquires a complex structure without a zero spatial harmonic because of the phase singularity on the optical axis. Spectrum broadening occurs mainly in the Stokes region.

2. Mathematical model

A numerical simulation of the problem of propagation of femtosecond pulses in fused silica was performed based on the self-consistent system of nonlinear differential equations. In the absence of initial noise, the stable-propagation distance of the optical vortex exceeds the nonlinear focusing length [17], due to which one can use the axisymmetric approximation in the initial stage of pulse propagation and filament formation by presenting the slowly varying light field amplitude in the form $E(r,\varphi,t,z) = A(r,t,z)\exp(\mathrm{i}m\varphi)$. Here, r is the transverse coordinate, t is time in the coordinate system travelling with a group velocity $v_g = (\partial k/\partial\omega)^{-1}|_{\omega=\omega_0}$, ω_0 is the centre frequency, z is the coordinate along the pulse propagation direction, and m is the topological charge.

The system of equations for the field $A(r,t,z)$ and free-carrier concentration $N_e(r,t,z)$ can be written as

$$2\mathrm{i}k_0\frac{\partial A}{\partial z} = \hat{T}^{-1}\left[\left[\frac{1}{r}\frac{\partial}{\partial r}\left(r\frac{\partial}{\partial r}\right) - \frac{m^2}{r^2}\right]A\right] + \hat{D}[A] + \frac{2k_0^2}{n_0}\hat{T}[\Delta n_K A]$$

$$+\frac{2k_0^2}{n_0}\hat{T}^{-1}[\Delta n_{pl}A] - \mathrm{i}k_0\sigma\hat{T}^{-2}[N_e A] - \mathrm{i}k_0(\alpha+\delta)A, \qquad (1)$$

$$\frac{\partial N_e}{\partial t} = R_E(I)(N_0 - N_e) + \nu_i(|A|^2)N_e - \beta N_e, \qquad (2)$$

where $k_0 = \omega_0 n_0/c = 2\pi n_0/\lambda_0$ is the wavenumber in the medium, $n_0 = 1.4533$ is the linear refractive index of fused silica [21], c is the speed of light in vacuum, and $\lambda_0 = 800$ nm is the centre wavelength.

The wave nonstationarity operator $\hat{T} = 1 - (\mathrm{i}/\omega_0)(\partial/\partial t)$ [20] is retained in Eqn (1) for the light field amplitude $A(r,t,z)$. The presence of this operator allows one to describe more accurately the increase in the slope of the pulse trailing edge under conditions of nonlinear self-focusing.

The dispersion operator is

$$\hat{D}[A] = \int_{-\infty}^{+\infty}\hat{T}_\Omega^{-1}[k^2(\omega_0+\Omega) - (k_0+k_1\Omega)^2]\tilde{A}\exp(\mathrm{i}\Omega t)\,\mathrm{d}\Omega \qquad (3)$$

where $\hat{T}_\Omega = 1 + \Omega/\omega_0$ is the spectral representation of the wave nonstationarity operator, $\Omega = \omega - \omega_0$ is the frequency detuning of the spectral component $\tilde{A}$, and $k_1 = (\partial k/\partial\omega)|_{\omega=\omega_0}$. The material dispersion is calculated according to the Sellmeier formula,

$$n(\omega) = \sqrt{1 + \sum_{i=1}^{3} C_i\frac{\omega_i^2}{\omega_i^2 - \omega_0^2}}, \qquad (4)$$

where the coefficients for fused silica in the vicinity of the centre wavelength are $C_1 = 0.6962$, $C_2 = 0.4079$, $C_3 = 0.8975$, $\omega_1 = 2.75\times10^{16}$ s^{-1}, $\omega_2 = 1.62\times10^{16}$ s^{-1}, and $\omega_3 = 1.90\times10^{14}$ s^{-1} [22].

The quantity Δn_K takes into account the change in the refractive index under the influence of Kerr nonlinearity:

$$\Delta n_K = (1-g)n_2 I(r,t) + g n_2\int_0^{+\infty} H(\tau)I(r,t-\tau)\,\mathrm{d}\tau, \qquad (5)$$

where $I = cn_0|A|^2/(8\pi)$ is the intensity, $n_2 = 3\times10^{-16}$ cm^2 W^{-1} is the cubic nonlinearity coefficient for fused silica [23], and $H(\tau)$ is a function describing the time-dependent nonlinear response of the medium. Calculations were performed within the instantaneous response approximation ($g = 0$).

The following quantities are used in the system of equations (1), (2):

$$\Delta n_{pl} = -\frac{\omega_{pl}^2}{2n_0\omega_0^2}, \quad \omega_{pl}^2 = \frac{4\pi e^2}{m_e}N_e, \qquad (6)$$

$$\sigma = \frac{2k_0}{n_0}\frac{1}{2n_0\omega_0^2}\frac{4\pi e^2}{m_e}\frac{\nu_{ei}}{\omega_0}, \qquad (7)$$

$$\alpha = \frac{Kh\omega_0}{I}R_E(I)(N_0 - N_e), \quad K = \left\langle\frac{U_i}{h\omega_0}\right\rangle + 1, \qquad (8)$$

$$\nu_i(|A|^2) = \frac{e^2\nu_{ei}}{2U_i m_e(\omega_0^2 + \nu_{ei}^2)}|A|^2. \qquad (9)$$

Here, Δn_{pl} is a nonlinear additive describing a decrease in the refractive index of the medium in the filament plasma channel; ω_{pl} is the plasma frequency; e is the elementary charge; m_e is the electron mass; σ is the inverse bremsstrahlung absorption cross section; α is the nonlinear absorption coefficient during photoionisation; K is the multiphotonity order; U_i = 9 eV is the band gap of fused silica [24]; $R_E(I)$ is the ionisation rate, which depends on the beam intensity and is calculated within the Keldysh model for condensed media [25] (the latter is successfully used to describe the experimental results on the filamentation of femtosecond radiation in fused silica [26]); $N_0 = 2.1\times10^{22}$ cm^{-3} is the concentration of neutral atoms [27]; the quantity $\nu_i(|A|^2)$ characterises the avalanche ionisation; and $\nu_{ei} = 10^{14}$ s^{-1} is the electron–ion collision frequency in fused silica [26]. The parameter δ describes the radiation

extinction in the medium; it was chosen to be 10^{-5} cm^{-1} [28]. The parameter $\beta = 10^{12}$ s^{-1} [29] characterises the free-carrier recombination.

To perform a comparative analysis during numerical simulation, we considered three initial conditions for the laser beam complex amplitudes in the case of a transform-limited Gaussian pulse:

$$A(r,t,z)|_{z=0} = A_G(r,t) = A_0 \exp\left(-\frac{r^2}{2r_0^2}\right)\exp\left(-\frac{t^2}{2t_0^2}\right) \quad (10)$$

for a Gaussian beam,

$$A(r,t,z)|_{z=0} = A_r(r,t) = \left(\frac{r}{r_0}\right)^2 A_G(r,t) \quad (11)$$

for an annular beam, and

$$A(r,t,z)|_{z=0} = A_v(r,t) = \exp(im\varphi)A_r(r,t) \quad (12)$$

for an annular beam with a phase singularity (optical vortex). Here, $r_0 = 50$ μm, $t_0 = 30$ fs, and $m = 2$.

The beam powers were chosen to be identical and equal to several critical powers for a beam with a phase dislocation:

$$P = 50P_{cr} = 6.25P_{crv}^{(2)}, \quad (13)$$

where $P_{cr} = 3.77\lambda_0^2/(8\pi n_0 n_2)$ [30] and $P_{crv}^{(2)}$ [16] are the critical powers of self-focusing for, respectively, a Gaussian beam and an annular beam with a phase singularity at $m = 2$. Their values in fused silica are approximately 2.7 and 21.6 MW, respectively. The critical power of self-focusing for the annular beam without a phase dislocation is close to P_{cr}.

The nonlinear equation describing the femtosecond laser pulse propagation (1) under the aforementioned initial conditions was numerically solved by the splitting method with respect to physical factors [31, 32]. To reduce the computation time, the program code was parallelised on multiprocessor computers.

3. Filamentation of an annular beam with a phase singularity

Let us consider the spatiotemporal dynamics and frequency-angular spectra of a pulse for an annular beam with a phase dislocation. Figure 1a shows the initial intensity distributions I for the pulse and the spectral power density S on the logarithmic scale.

The intensity peak for the annular beam [see (12)] with a magnitude of about 4.6×10^{11} W cm^{-2} is located at a distance of about 70 μm from the optical axis. The frequency-angular spectrum has a bimodal structure with a zero spatial harmonic (due to the phase singularity) and a maximum at the centre wavelength $\lambda_0 = 800$ nm.

In the initial stage of beam propagation in fused silica, the beam retains its annular structure (Fig. 1b); at the same time, due to the radiation self-focusing, the width of the annular structure in the central part of the pulse is significantly reduced. This transformation of the pulse is accompanied by broadening of its angular and frequency spectra.

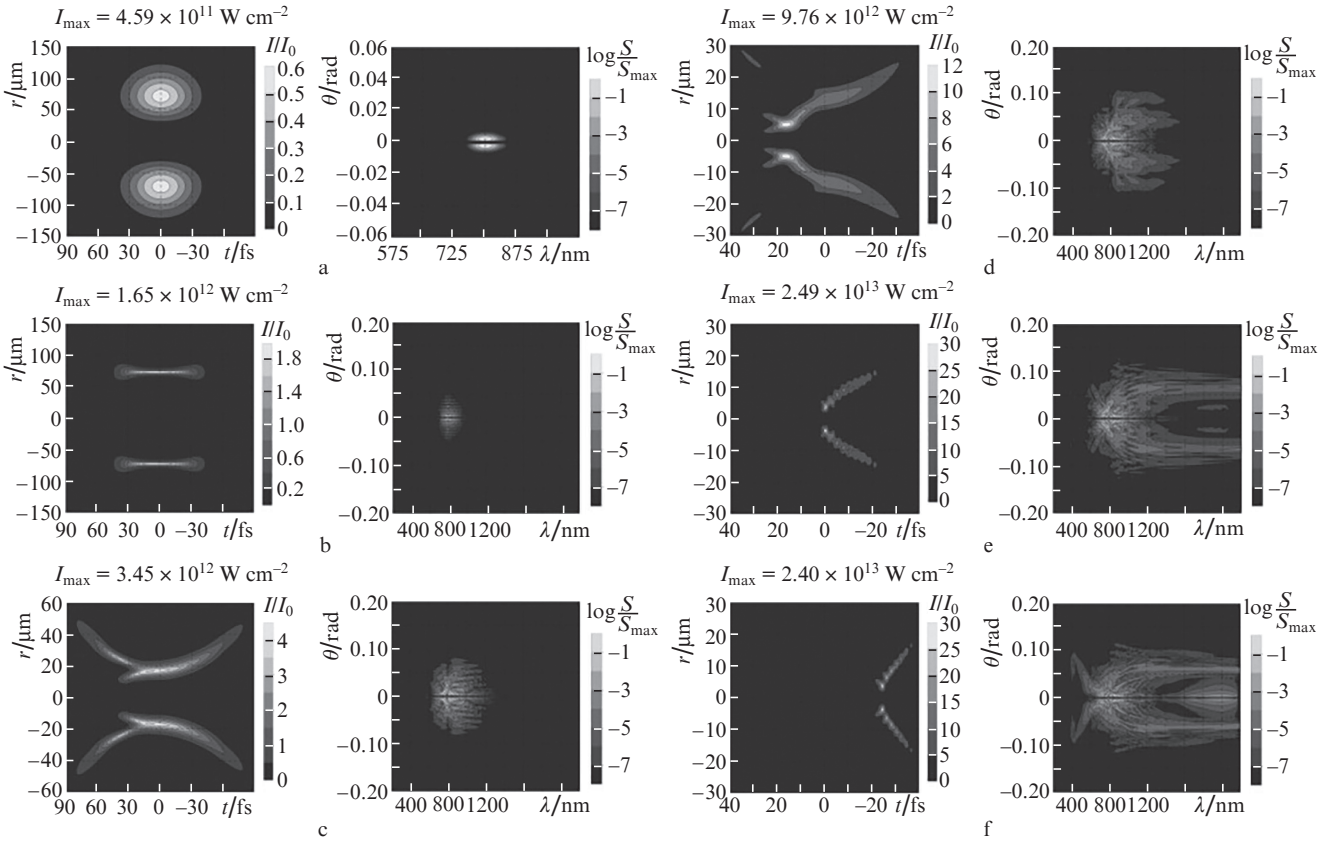

Figure 1. Spatiotemporal distributions of intensity I and frequency-angular spectra S for the filamentation of an annular beam with a phase singularity at distances z = (a) 0, (b) 0.43, (c) 1.05, (d) 1.08, (e) 1.11, and (f) 1.15 cm; the angle θ is counted from the optical axis.

As the pulse propagates further, the energy of its central temporal layers tends to flow from the beam periphery to the optical axis, which is mainly due to the influence of diffraction. In the absence of nonlinearity, the annular beam diffraction leads to the formation of a unimodal structure with a maximum located on the optical axis, which then broadens. The presence of a phase singularity on the axis impedes the formation of this structure, and the beam is diffracted retaining its annular shape, while the radius of the ring in the pulse centre is reduced. Due to a decrease in the group velocity of the temporal layers affected by the Kerr nonlinearity, the maximum of the intensity begins to shift from the centre of the pulse to its trailing edge; the more rapidly this shift occurs, the stronger the beam is self-focused. In this stage, the frequency spectrum broadens mainly towards the Stokes region.

At the instant when the maximum intensity exceeds the initial one by a factor of 4–5, the plasma formation threshold is reached, and the density of electrons formed in the medium becomes sufficient to suppress the Kerr self-focusing in the next pulse layers. Under these conditions, due to the plasma-induced defocusing of the rear part of the pulse and sharpening of its trailing edge, one can observe splitting of the annular structure in two directions: to the beam periphery and to the beam axis. This process is accompanied by a significant broadening of the spatial spectrum (Fig. 1c). Fringes caused by the interference from point radiation sources arise in the frequency-angular spectrum of the pulse [33].

When the peak intensity approaches values of $\sim 10^{13}$ W cm^{-2}, the corresponding region of the pulse begins to shift to its leading edge, because the plasma nonlinearity considerably defocuses the tail part (Fig.1d). The spatiotemporal structure exhibits low-intensity cones in both the front and rear temporal layers; these cones are residuals after the previous self-action. Because of the increased field gradients in space, the angular spectrum is broadened even stronger, and the fringes in it become wider and less pronounced.

Since the phase dislocation is retained during self-action, and the field on the beam axis is absent, the energy flow to the axis ceases during further pulse propagation (Fig. 2). The filament formed by this instant, jointly with its plasma channel, is shaped as a ring (Fig. 1e) with a radius of 3–4 μm. The spatial distribution of the pulse intensity is a set of rings, whose radius increases when moving from the centre of the pulse to its front. The rings in the front part of the pulse are due to the interference of the radiations from the periphery (which continues to be focused) and the defocused central part of each temporal layer. The structure of the frequency-angular spectrum is complicated; one can observe broadening towards both the Stokes and anti-Stokes regions. Qualitatively, this pattern is retained at a distance of several hundreds of micrometers.

The intensity maximum continues to be shifted toward the pulse front without any significant changes in the spatiotemporal dynamics (Fig. 1f). The peak intensity is stabilised at a level of $\sim 2.4 \times 10^{13}$ W cm^{-2}; the plasma density under these conditions is $\sim 10^{20}$ cm^{-3}. Conical emission becomes pronounced in the anti-Stokes region of the frequency-angular spectrum.

The distribution of the fluence for an annular beam with a phase singularity in the vicinity of the filament onset is presented in Fig. 2. One can clearly see a region with a close-to-zero fluence (several micrometres in size) on the optical axis, around which a region of a maximum fluence was formed. Solid lines show the ring boundaries in the nonlinear regime; the ring radius was determined from the maximum of the fluence. The dashed lines correspond to the case where an annular beam with a phase singularity (with an initial radius coinciding with the radius of the annular structure in the nonlinear case at $z = 1.09$ cm) undergoes linear diffraction. It can be seen that the ring diffuses under the diffraction, whereas a quasi-waveguide regime of beam propagation (which can be referred to as an annular filament) is maintained in the nonlinear medium.

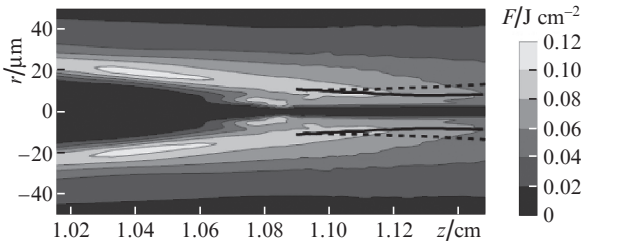

Figure 2. Fluence F as a function of distance z along the pulse propagation direction in the vicinity of the filament start point.

4. Analysis of the filamentation of beams with different profiles

Let us compare the specific features of filamentation of an annular beam with a phase singularity [see (12)] with the features of filamentation of a unimodal Gaussian beam [see (10)] and an annular beam free of phase singularity [see (11)].

Numerical simulation was performed for the same radiation power (13) and parameters $r_0 = 50$ μm and $t_0 = 30$ fs. The filament start was chosen to be the point where the pulse peak intensity reaches the first local maximum; this configuration corresponds to the local balance between the Kerr self-focusing and plasma defocusing, which is typical of filaments. The peak intensity in the filament for all three beams is $(2-4) \times 10^{13}$ W cm^{-2}. Depending on the beam shape, the filament start point is located at significantly different distances. In the case of a Gaussian beam, the peak power exceeds the critical value by a factor of 50, and the self-focusing of the pulse central layers very rapidly leads to the filament formation (at a distance of $z = 0.21$ cm), whereas the annular beam of the same power is first focused into a ring with an intensity elevated by a factor of no more than 5 and only then, as the annular structure is compressed, the intensity increases and a plasma channel is formed in the beam.

The spatiotemporal dynamics of annular beams in the initial stage of self-action is qualitatively similar (Fig. 3a); however, the energy flow to the optical axis for the beam with a phase dislocation occurs more slowly, and, at each distance z, the ring radius for the optical vortex somewhat exceeds that for the conventional annular beam. For the beam free of singularity, the intensity maximum in the nonlinear focus arises on the optical axis, and the presence of a phase vortex leads to focusing into a ring (Fig. 3b). As the annular beam propagates further, the nonlinear focus is displaced to the front temporal layers; this transfer is accompanied by the formation of interference rings behind them, which are of the same nature as the concentric cones formed during the Gaussian beam filamentation (Fig. 3c). The pulse rear layers on the beam axis, which are defocused by plasma, interfere with the

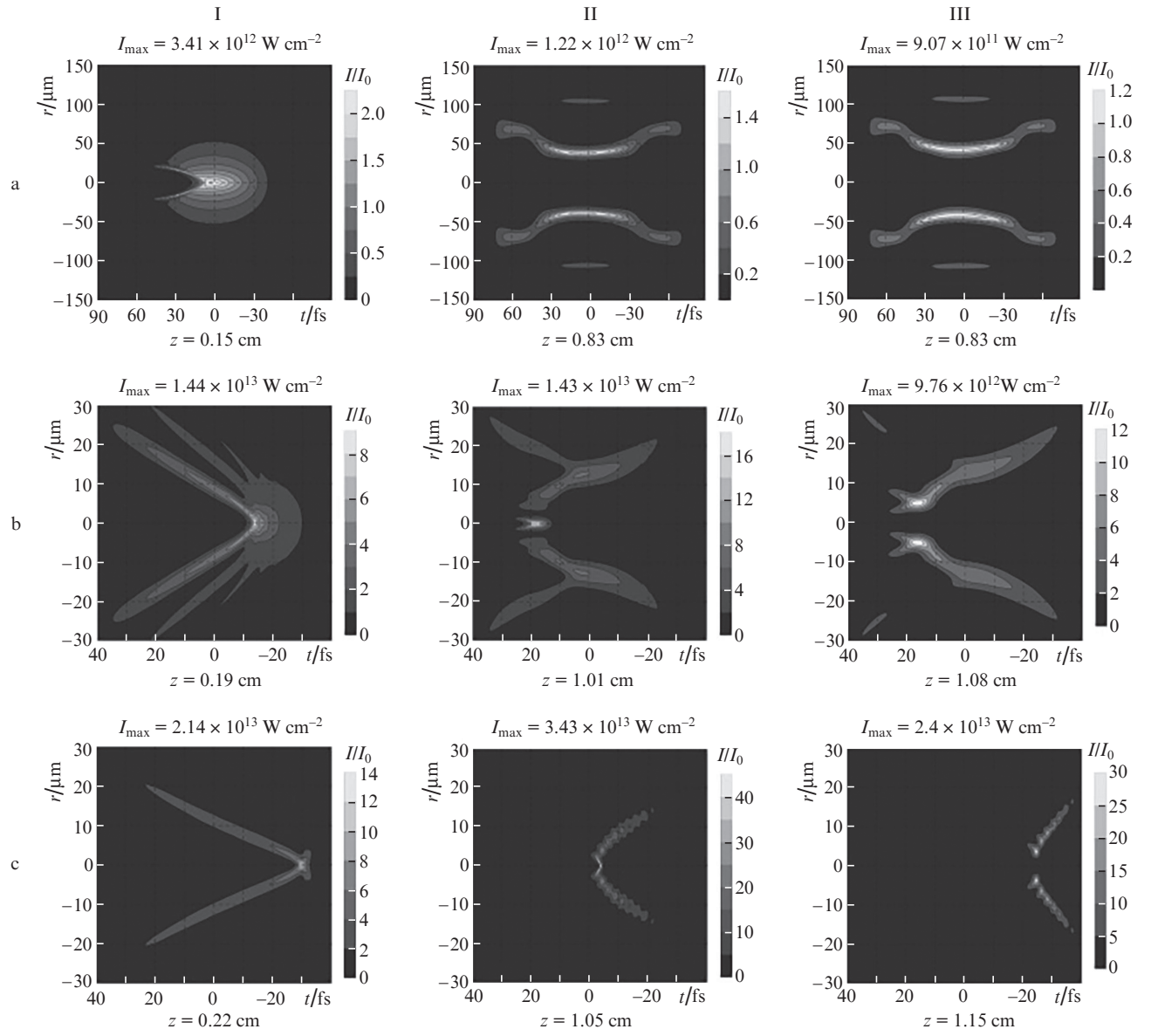

Figure 3. Spatiotemporal intensity distributions during the filamentation of (I) a Gaussian beam, (II) an annular beam without a phase singularity, and (III) an optical vortex at different pulse propagation distances z.

pulse periphery, which continues to be focused. In the case of the optical vortex, a chain of local maxima is also formed; they are due to the energy flux redistribution along the directions toward the optical axis and away from it. In a Gaussian beam, in contrast to annular beams, a nonlinear focus is formed at the pulse centre and then rapidly moves to its leading edge; this behaviour is related to the plasma defocusing, which begins to manifest itself in the early stage of self-action.

The frequency-angular spectra of annular beams have a complex structure (see Fig. 4). They are qualitatively similar; however, the presence of a phase singularity on the beam axis leads to the absence of the zero spatial harmonic, in particular, during the self-action.

In the wavelength range above 1200 nm, the angular spectral broadening of annular beams is more homogeneous, whereas a Gaussian beam exhibits pronounced conical emission with a divergence angle of about 4°. In contrast, in the anti-Stokes wavelength range (400–700 nm), the conical emission is more pronounced for the optical vortex; here, the radiation divergence angle increases with decreasing wavelength.

To estimate quantitatively the energy redistribution from the central part of the spectrum to the neighbouring regions during the beam filamentation, we will arbitrarily select three spectral regions: anti-Stokes (λ < 760 nm), central ($\lambda \in$ [760 nm, 840 nm]), and Stokes (λ > 840 nm) (Fig. 5).

Initially all the beams under consideration have approximately the same spectral width: almost 100% energy is concentrated in the range of 800 ± 40 nm. During the propagation of the annular beam at a distance larger than 1 cm, a large part (about 30%) of its energy is transferred to the Stokes region, and a much smaller part (less than 5%) is transferred to the anti-Stokes region. In the Gaussian beam, at distances up to z = 0.3 cm, about 90% of energy remains in the central spectral region and only about 10% of energy is transferred to the long-wavelength part of the spectrum. For

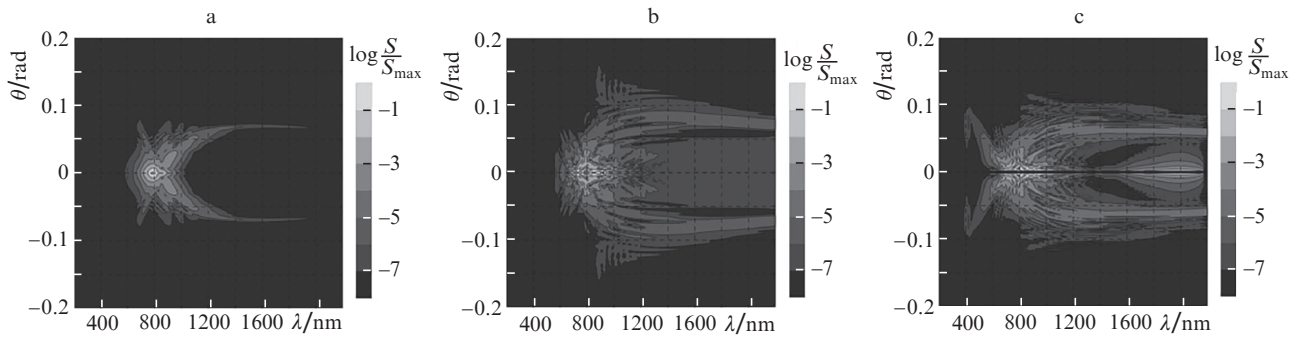

Figure 4. Frequency-angular spectra S for the filamentation of (a) a Gaussian beam, (b) an annular beam free of phase dislocation, and (c) an optical vortex; the distance from the filament start point is 0.06 cm.

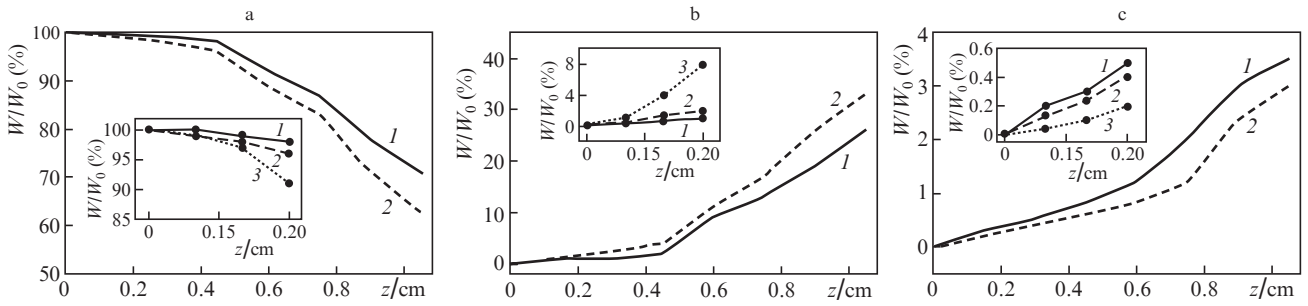

Figure 5. Redistribution of energy W from (a) the central spectral region to (b) the Stokes and (c) anti-Stokes regions in annular beams (*1*) with and (*2*) without a phase dislocation. The insets show also the data for (*3*) a Gaussian beam.

the beam with a phase dislocation, as compared with a conventional annular beam, the energy rise is more efficient in the anti-Stokes region and less efficient in the Stokes region; as a result, the energy transfer from the central spectral region is significantly slowed down.

5. Conclusions

The self-action of an annular beam with a phase singularity in fused silica at a wavelength of 800 nm may lead to the formation of a structure with a cross section in the form of a ring with radius of 3–4 μm and width of 1–2 μm, respectively, and a peak intensity of $(2.0–2.5) \times 10^{13}$ W cm^{-2}. This tubular structure can be referred to as a filament, because it is retained at a distance of no less than ten diffraction lengths and forms a plasma channel behind it; this channel is also tubular, and the maximum electron concentration in it is 10^{20} cm^{-3}. The dynamics of the frequency-angular spectrum of an annular beam with a phase singularity is similar to that of the spectrum of a conventional annular beam (except for the absence of the zero spatial harmonic). During the optical vortex filamentation, about a third of the energy may be redistributed to the Stokes region and a much smaller part of the energy may be transferred to the anti-Stokes region. The contrast of the conical emission in the Stokes region is much worse as compared with a Gaussian beam.

Acknowledgements. This work was supported by the Russian Foundation for Basic Research (Grant No. 14-22-02025) and by the Grants Council of the President of the Russian Federation for Support of Leading Scientific Schools (Grant No. NSh-9695.2016.2).

References

1. Kandidov V.P., Shlenov S.A., Kosareva O.G. *Kvantovaya Elektron.*, **39**, 205 (2009) [*Quantum Electron.*, **39**, 205 (2009)].
2. Couairon A., Mysyrowicz A. *Phys. Rep.*, **441**, 47 (2007).
3. Kasparian J. *American Scientist*, **94**, 150 (2006).
4. Liu W., Chin S.L. *Opt. Express*, **13**, 5750 (2005).
5. Tzortzakis S., Sudrie L., Franco M., Prade B., Mysyrowicz A., Couairon A., Berge L. *Phys. Rev. Lett.*, **87**, 213902 (2001).
6. Kasparian J., Wolf J.-P. *Opt. Express*, **16**, 466 (2008).
7. Tzortzakis S., Anglos D., Gray D. *Opt. Lett.*, **31**, 1139 (2006).
8. Chateauneuf M., Payeur S., Dubois J., Kieffer J.-C. *Appl. Phys. Lett.*, **92**, 091104 (2008).
9. Yamada K., Watanabe W., Toma T., Itoh K., Nishii J. *Opt. Lett.*, **26**, 19 (2001).
10. Kruglov V.I., Logvin Yu.A., Volkov V.M. *J. Mod. Opt.*, **39**, 2277 (1992).
11. Vincotte A., Berge L. *Phys. Rev. Lett.*, **95**, 193901 (2005).
12. Volyar A.V., Fadeeva T.A., Egorov Yu.A. *Pis'ma Zh. Tekh. Fiz.*, **28**, 70 (2002).
13. Volyar A.V., Fadeeva T.A. *Opt. Spektrosk.*, **94**, 264 (2001).
14. Blonskyi I.V., Kadan V.M., Dergachev A.A., Shlenov S.A., Kandidov V.P., Puzikov V.M., Grin L.O. *Ukr. J. Phys.*, **58**, 341 (2013).
15. Bigelow M.S., Zerom P., Boyd R.W. *Phys. Rev. Lett.*, **92**, 083902 (2004).
16. Vuong L.T., Grow T.D., Ishaaya A., Gaeta A.L., Hooft G.W., Eliel E.R., Fibich G. *Phys. Rev. Lett.*, **96**, 133901 (2006).
17. Vlasov R.A., Volkov V.M., Dedkov D.Yu. *Kvantovaya Elektron.*, **43**, 157 (2013) [*Quantum Electron.*, **43**, 157 (2013)].
18. Neshev D.N., Dreischuh A., Maleshkov G., Samoc M., Kivshar Y.S. *Opt. Express*, **18**, 18368 (2010).
19. Hansinger P., Dreischuh A., Paulus G.G. *Appl. Phys. B*, **104**, 561 (2011).
20. Brabec T., Krausz F. *Phys. Rev. Lett.*, **78**, 3282 (1997).
21. Weber M.J. *Handbook of Optical Materials* (Boca Raton: CRC Press, 2003).
22. Malitson I.H. *J. Opt. Soc. Am.*, **55**, 1205 (1965).

23. Milam D. *Appl. Opt*., **37**, 546 (1998).
24. Lenzner M., Kruger J., Sartania S., Cheng Z., Spielmann Ch., Mourou G., Kautek W., Krausz F. *Phys. Rev. Lett*., **80**, 4076 (1998).
25. Keldysh L.V. *Zh. Eksp. Teor. Fiz*., **47**, 1945 (1964).
26. Couairon A., Sudrie L., Franco M., Prade B., Mysyrowicz A. *Phys. Rev. B*, **71**, 125435 (2005).
27. Lide D.R. *Handbook of Chemistry and Physics* (Boca Raton: CRC Press, 2005).
28. Listvin A.V., Listvin V.N., Shvyrkov D.V. *Opticheskie volokna dlya linii svyazi* (Optical Fibres for Communication Lines) (Moscow: Velkom, 2002).
29. Audebert P., Daguzan Ph., Dos Santos A., Gauthier J.C., Geindre J.P., Guizard S., Hamoniaux G., Krastev K., Martin P., Petite G., Antonetti A. *Phys. Rev. Lett*., **73**, 1990 (1994).
30. Chiao R.Y., Garmire E., Townes C.H. *Phys. Rev. Lett*., **13**, 479 (1964).
31. Fleck J.A., Morris J.R. *Appl. Phys*., **10**, 129 (1976).
32. Marchuk G.I. *Metody vychislitel'noi matematiki* (Methods of Computational Mathematics) (Moscow: Nauka, 1980).
33. Dormidonov A.E., Kandidov V.P. *Laser Phys*., **19**, 1993 (2009).